Current spread and overheating of high power laser bars

B. Laikhtman[a)]
Power Photonic, 214 Old Chemistry, Stony Brook, New York 11794-3717

A. Gourevitch, D. Donetsky, D. Westerfeld, and G. Belenky
Department of Electrical Engineering, State University of New York at Stony Brook, Stony Brook, New York 11794

(Received 27 May 2003; accepted 12 January 2004)

The heating of a semiconductor laser bar imbedded between two heat spreaders has been studied theoretically and experimentally. The model included the p-cladding layer, active region, n-cladding layer, and n-substrate. Heat sources from the active region and both cladding layers were considered. An analytical relation was obtained between the temperature distribution in the laser and the bar geometry. The analytical approach revealed features that are usually missing in purely numerical modeling. It was shown that the current density across the active region is nonuniform, and that the magnitude of the nonuniformity grows when the resistance of the p-cladding layer decreases. This nonuniform current distribution can lead to higher temperatures at the edges of the laser stripe than in the middle. It was found that mutual heating of the individual lasers in the bar is controlled mainly by the overlap of the temperature fields in the heat spreaders. The theoretical results obtained without any fitting parameters show good agreement with the experimentally measured dependence of the active region temperature on pumping current. © *2004 American Institute of Physics.* [DOI: 10.1063/1.1655687]

I. INTRODUCTION

High-power infrared diode laser arrays are effective sources for pumping solid-state lasers.[1–3] These laser arrays are composed of one or more laser bars; each laser bar consists of numerous individual laser emitters formed on a single piece of semiconductor. There are a number of factors that limit the output power and reliability of diode lasers, for example, catastrophic optical damage and overheating. For the 1.5 μm InGaAsP/InP lasers used in this experiment, the output power and reliability are limited mainly by overheating. A deep understanding of all overheating mechanisms can facilitate further progress with these lasers.

The purpose of the present article is to study the temperature rise (overheating) in the laser structure induced by power dissipation in the active region, p- and n-cladding layers, and the substrate. The analysis was developed for single-emitter lasers, but much of it is directly applicable to multi-emitter broad-area laser bars.

Previous theoretical work considered the temperature distribution along the laser cavity,[4,5] the temperature distribution in the direction perpendicular to the layers of the structure,[6,7] and the facet heating[4,5,8] (see also the review by Erbert *et al.*[9]). The first studies of the temperature profile in the lateral direction[10,11] were based on the assumption of uniform heat sources. In this article, we consider a more realistic and complicated model, including nonuniform lateral current distribution.

In previous publications, the current density was sometimes calculated under the assumption that it was constant at the contact stripe and falls off as the square of the distance away from the contact.[12–17] An exact analytical solution to the Laplace equation that controls the current spread when carrier diffusion can be neglected was obtained by Lengyel *et al.*[18] They studied a narrow stripe geometry in which the width of the stripe is of the order of its distance from the active region. Similar models have been considered by Wilt,[19] Joyce,[20] and Agrawal.[21] A comprehensive comparison of these models has been made by Papannareddy *et al.*[22] The geometry considered by Lengyel *et al.*[18] corresponds to the situation encountered in ridge lasers. For high-power lasers, the width of the stripe is much larger than the cladding thickness, and the substrate thickness is comparable to the stripe width. In the present article, it is shown that this geometry leads to a high current density near the edges of the active region.

We have considered a structure typical of broad-area lasers. We found an analytical expression for the current density in the lateral direction. From the current density, we determined the resulting heat sources, and we then analytically solved the heat conduction equation for the whole system, taking into account the thermal resistance of the layers separating the laser structure from the heat sinks. Experimental results obtained using a high-power 1.5 μm InP-based laser array demonstrated good agreement between the theoretical results and the measured laser temperature.

The structure of the article is as follows. In Sec. II, we describe the model and present a picture of relevant phenomena and qualitative results. Sections III and IV contain the main points of the calculations of the current spread and temperature distributions, respectively. In Sec. V, we present the results of the calculations and compare them with experiment, followed by the conclusion.

[a)]Permanent address: Racah Institute of Physics, Hebrew University, Jerusalem, 91904, Israel; electronic mail: borisl@atrg.com

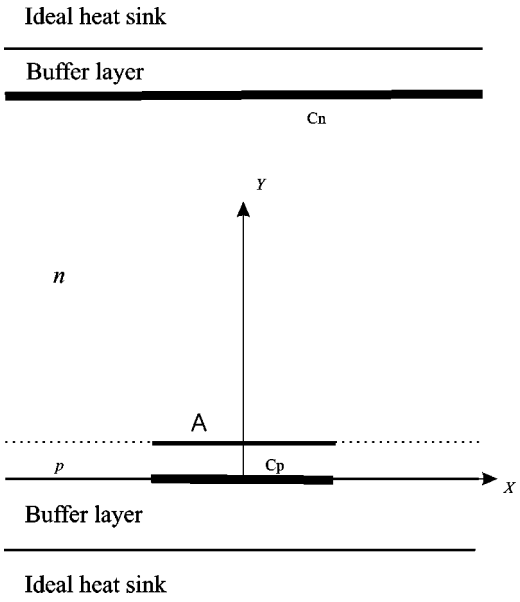

FIG. 1. The structure of the laser. The n-layer consists of a thin n-cladding and n-substrate. C_p and C_n are p- and n-contacts, A is the active region.

II. MODEL

The temperature field in an array of lasers is the sum of the fields produced by each laser emitter separately. For this reason, we start the analysis using a theoretical model that contains only one laser emitter (Fig. 1). The lasing heterostructure consists of a p-contact stripe C_p, a p-cladding layer, an active region A, an n-cladding layer, the substrate, and an n-contact C_n. We consider a cooler design in which the heat is removed from both the p- and n-sides. Typically, a water-cooled microchannel heat sink is used for high-power laser arrays. We assume that such a heat sink is ideal, and it is connected to the laser structure via two buffer layers with finite thermal resistance.

The length of the laser cavity is generally much larger than the stripe width and the thickness of the whole structure. This allows us to neglect the effect of facets while studying the temperature distribution far from the ends of the cavity. Thus, we reduced a three-dimensional problem for electric potential and temperature field to a two-dimensional one that facilitated analytical solution. The laser structure that we used in the calculation was typical in that the p-cladding thickness b_1 was small compared to the width of the stripe a and the total thickness of n-cladding and substrate, $b-b_1$. Here, b is the distance between the p- and n-contacts. We considered a and b of the same order. The thickness of the active region, which includes the quantum wells (QWs) and a relatively lightly doped waveguide, is a few hundred Å, which is significantly smaller than b_1. For this reason, we neglected the active region thickness and considered this region as an interface between the p- and n-regions. We also assumed a uniform doping of the p- and n-regions and characterized them by electrical conductivities σ_p and σ_n, respectively, and the same thermal conductivity κ.

We considered laser operation above threshold and with only moderate overheating. Under these conditions, we can assume that the voltage drop across the active region (U_0) remains constant while the voltage across the p- and n-layers increases with current. Our problem is to calculate the temperature distribution in the structure and specifically in the active region as a function of the total current, given the geometry of the structure, all necessary physical parameters, U_0, the threshold current, and the differential efficiency.

Throughout the article we use analytical approaches, leaving numerical calculation for the last stage (evaluation of integrals). The advantage of analytical calculation as compared to numerical calculation is that the result contains symbolic parameters, such as a, b, σ_n, σ_p, etc. A reader who wants to calculate the temperature distribution in another structure needs only to substitute the parameters of the structure in the final expressions. Using a numerical approach, the calculation for a new structure requires the repetition of the calculation with the help of a program that may not be accessible to the reader. In addition, an analytical result allows one to understand the qualitative dependence of device characteristics on the parameters without performing time-consuming calculations. A disadvantage of the analytical approach is that analytical solutions can be obtained only for rather simple models, for example, we assumed that the conductivity σ_n does not change across the whole n layer, which is equivalent to a uniform doping. Fortunately, relations between typical geometrical parameters are such that many of the complications of real laser heterostructures lead to small effects that are beyond the accuracy of experiments and can be neglected for the first approximation. Taking this into consideration, we use small parameters to obtain analytical solutions to both the electric and the thermal problems.

The first use of a small parameter comes from very high doping of both the p- and n-layers, which leads to a screening length smaller than all characteristic lengths (e.g., the thickness of the p-cladding). This strong screening greatly reduces the concentration gradients in both the p- and n-regions that would create an electric field. This leads to reduction of the diffusion current, and with very good accuracy, the diffusion current can be neglected compared to the drift current. As a result, the current distribution is controlled by the Laplace equation for the electric potential. We obtained an analytical solution to this equation in the region including the p-cladding, the n-cladding, and the substrate. It is well known that the electric field is singular near sharp edges of a conductor. As a result, the current density near the edges of the contact stripe is significantly larger than at the middle. The effects of this singularity also appeared in our solution, leading to a higher current density near the edges of the active region, as seen in Figs. 2 and 3. The effect is weakened because the higher current near the edges leads to a higher potential drop between the stripe and the active region edges, which smears the singularity. The lateral current spread takes place mainly in the n-layer because its thickness is comparable with the width of the stripe. The lateral current spread in the p-cladding is negligible because of its very small thickness compared to the width of the stripe.

To simplify the solution of the thermal problem, we considered the buffer layer as a thermal resistance of the boundary between the laser structure and the ideal heat sink. In

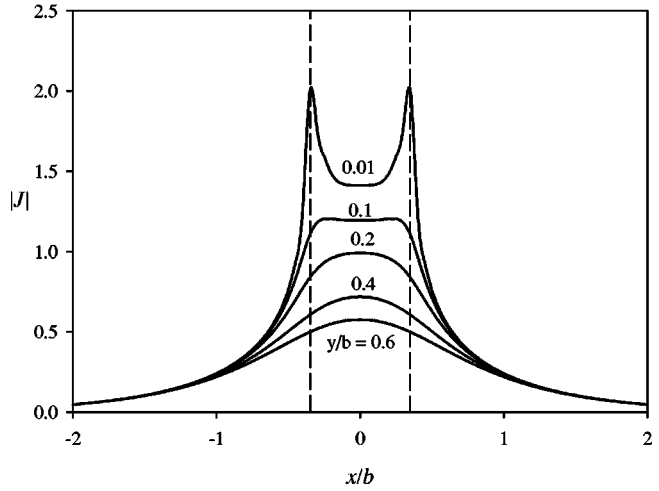

FIG. 2. The dimensionless current density (in units of I/Lb, where I is the total current, L is the cavity length, and b is the thickness of the structure) as a function of x/b given y. The ratio of the p- and n-layer resistances is $b_1\sigma_n/b\sigma_p=4$. The numbers on the curves are dimensionless distances from the active region, y/b. The edges of the active region as shown by the dashed lines correspond to $x/b=\pm 0.357$. Singularities of the current near the edges of the stripe are very pronounced at small y/b and disappear with the growth of y. The lateral spread of the current does not grow much even at large y/b, close to the n-contact.

reality, a significant part of the heat spread in the lateral direction takes place in the bulk of the buffer layer. A detailed discussion of the heat spread in the buffer layer is given elsewhere.[3] In this work, we considered the heat spread only in the laser structure.

The high current density near the edges of the active region leads to greater heating there. This effect competes with better cooling conditions: the current density drops very quickly in the lateral direction away from the active region, and the material there is not heated. As a result, for small p-cladding resistance, the edges of the active region have

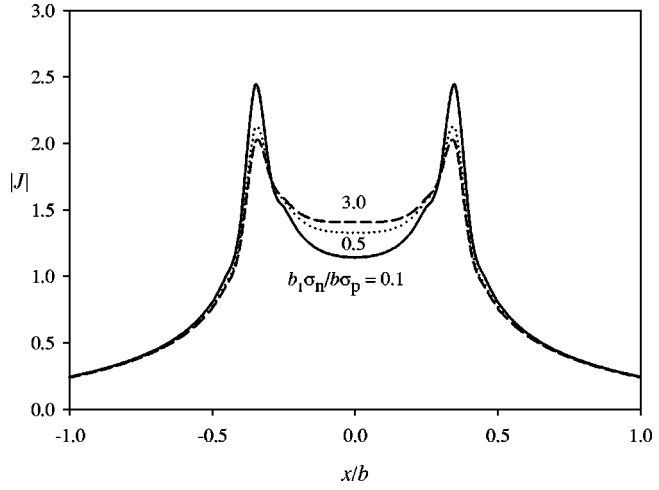

FIG. 3. The dimensionless current density (in units of I/Lb, where I is the total current, L is the cavity length, and b is the thickness of the structure) as a function of x/b for different p-cladding resistances. The edges of the active region correspond to $x/b=\pm 0.357$. The distance from the p-contact $y=b_1=0.01b$, the numbers on the curves are the values of the ratio of the p- and n-layer resistances, $b_1\sigma_n/b\sigma_p$. The smaller this parameter is, the more pronounced are the singularities at the edges of the stripe.

higher temperature than its middle, while, when the resistance of p-cladding is large, the temperature in the middle is higher.

The lateral heat spread is determined by the geometrical parameters of the structure and the ratio of the thermal resistances of the buffer layer and the structure. We consider the regime of moderate current when most of the dissipated power comes from the active region. Because the active region is much closer to the p-contact than to the n-contact, the active region is cooled mainly from the p-side. If the thermal resistance of the buffer layers were zero, the heat would spread laterally away from the active region at a distance on the order of b_1. A finite thermal resistance of the buffer layer makes this distance larger. The heat generated in the relatively thick n-layer spreads over a significantly wider region. This is of little practical concern because the amount of heat generated in n-layer is relatively small.

In our model, the magnitude of the laser overheating depends strongly on the thermal resistance of the thermal buffers that separate the laser structure from the ideal heat sink. When this thermal resistance is zero, the overheating is very small.

In the next two sections, this qualitative description is supported by quantitative calculation that allow us to present a complete picture of the temperature distribution inside the laser structure.

III. CURRENT SPREAD

The calculation of the current spread is hindered by the fact that the structure consists of two layers with different conductivities. The small thickness of the p-cladding (b_1), compared to the width of the contact (a), however, allows us to assume the current spread in the p-cladding is negligible. The potential drop across this layer is $U_p(x)=b_1 j_y(x,0)/\sigma_p$, where $j_y(x,y)$ is the component of the current density across the layer. The potential at the contact stripe U is constant, and the potential drop across the active region U_0 is also constant above threshold. However, the potential at the n-side of the active region,

$$U_a(x)=U-U_0-b_1 j_y(x,0)/\sigma_p, \tag{3.1}$$

depends on the distribution of $j_y(x,0)$. The approximation Eq. (3.1) is not valid in a small vicinity of the edges of the active region. We discuss this problem at the end of Sec. III B.

First, we find the electric potential in the n-layer, assuming that the potential $U_a(x)$ is known and that the normal current across the $p-n$ interface $j_y(x,0)=0$ away from the active region. The other boundary condition for the n-layer is zero potential at the n-contact. The solution to this problem is given in Sec. III A. This solution allows us to find the current density $\boldsymbol{j}(x,y)$ everywhere in the n-layer and, in particular, the current density normal to the $p-n$ interface, $j_y(x,0)$, at $|x|<a/2$. This current density depends on $U_a(x)$ and substitution of it in Eq. (3.1) provides an integro-differential equation for $U_a(x)$. This equation is solved in Sec. III B. This completes the calculation of the current density in the structure.

A. Current spread in the *n*-layer

The current density $\boldsymbol{j}(x,y)$ can be found from current conservation $\nabla\cdot\boldsymbol{j}=0$ and Ohm's law, $\boldsymbol{j}=-\sigma_n\nabla\phi$, where ϕ is the electric potential. The carrier concentration is typically large, which allows us to neglect the diffusion current. Then,

$$\nabla^2\phi=0. \tag{3.2}$$

The boundary conditions for Eq. (3.2) are

$$y=0,\ |x|<a/2:\quad \phi=U_a(x), \tag{3.3a}$$

$$y=0,\ |x|>a/2:\quad \frac{\partial\phi}{\partial y}=0, \tag{3.3b}$$

$$y=b:\quad \phi=0. \tag{3.3c}$$

In addition, the potential goes to zero when $|x|$ goes to infinity. It follows from the symmetry of the problem that $U_a(-x)=U_a(x)$. To simplify the notation, we chose $y=0$ in this section to be the level of the active region.

The mixed boundary conditions at $y=0$ do not allow us to use separation of variables for the solution of Eq. (3.2), so that we must make use of a more powerful method: conformal mapping. According to this method, ϕ can be considered as the real part of an analytic function of the complex variable $z=x+iy$:

$$\chi(z)=\phi(x,y)+i\psi(x,y). \tag{3.4}$$

The problem now is to find the function $\chi(z)$ analytic in the stripe $0<y<b$ that satisfies the boundary conditions

$$y=0,\ |x|<a/2:\quad \phi=U_a(x), \tag{3.5a}$$

$$y=0,\ |x|>a/2:\quad \psi=\text{const}, \tag{3.5b}$$

$$y=b:\quad \phi=0. \tag{3.5c}$$

Eq. (3.5b) follows from Eq. (3.3b) due to Cauchy–Riemann conditions

$$\frac{\partial\phi}{\partial x}=\frac{\partial\psi}{\partial y},\quad \frac{\partial\psi}{\partial x}=-\frac{\partial\phi}{\partial y}, \tag{3.6}$$

that provide the analytic property of $\chi(z)$.

The boundary problem for the stripe (3.5) can be reduced to a problem in the upper half-plane of another complex variable $w=u+iv$, where its solution is simpler. This is done with the transformation

$$w=\tanh\frac{\pi z}{2b},\quad z=\frac{b}{\pi}\ln\frac{1+w}{1-w}. \tag{3.7}$$

This transformation maps the segment of the real axis $|x|<a/2$ to the segment of the real axis $|u|<u_a$, where $u_a=\tanh(\pi a/4b)$. The negative and positive parts of the real axis outside of this segment are mapped to the parts of the real axis where $-1<u<u_a$ and $u_a<u<1$, respectively. The parts with $x<0$ and $x>0$ of line $y=b$ are mapped to the regions of the real axis where $u<-1$ and $u>1$, respectively, so that the point $z=ib$ is mapped to infinity at w-plane. Now the problem is to find the function $\chi(w)$ analytic in the upper half-plane of w and satisfying the following conditions at the real axis:

$$|u|<u_a:\quad \phi=(U-U_0)\Phi(u), \tag{3.8a}$$

$$u_a<|u|<1:\quad \psi=\text{const}, \tag{3.8b}$$

$$1<|u|:\quad \phi=0, \tag{3.8c}$$

where

$$\Phi(u)=\frac{1}{U-U_0}U_a\left(\frac{b}{\pi}\ln\frac{1+u}{1-u}\right). \tag{3.9}$$

Additional conditions are continuity of $\phi(u,v)$ near singular points of the transformation $w=u_a$, $w=1$, and a decrease of $\phi(u,v)$ to zero when w goes to infinity. Apparently, $\Phi(-u)=\Phi(u)$.

The difficulty of the problem is that boundary conditions (3.8) are mixed, that is, at some parts of the boundary only the real part of $\chi(w)$ is given, while at the others only the imaginary part is known. The problem can be solved with the Keldysh–Sedov method,[23] and the result is

$$\chi(w)=-\frac{2(U-U_0)}{\pi}w\sqrt{(1-w^2)(w^2-u_a^2)}\times\left[\int_0^{u_a}\frac{\Phi(t)}{\sqrt{(1-t^2)(u_a^2-t^2)}}\frac{dt}{t^2-w^2}-\frac{\Pi\left(-\frac{1-u_a^2}{1-w^2},\sqrt{1-u_a^2}\right)}{(1-w^2)\boldsymbol{K}(\sqrt{1-u_a^2})}\int_0^{u_a}\frac{\Phi(t)dt}{\sqrt{(1-t^2)(u_a^2-t^2)}}\right], \tag{3.10}$$

where $\boldsymbol{K}(k)$ and $\Pi(s,k)$ are complete elliptic integrals of the first and the third kind, respectively.

The total current across the device can be easily calculated by the integration of the current density at $y=0$ with the help of Eq. (3.6):

$$I=-L\int_{-a/2}^{a/2}j_y dx=2L\sigma_n\psi(x=a/2,\,y=0)=2L\sigma_n\psi(u_a,0), \tag{3.11}$$

where L is the length of the stripe. The value of $\psi(u_a,0)$ is obtained in the boundary problem for the potential, and the result is

$$I=\frac{U-U_0}{r},\qquad r=\frac{\boldsymbol{K}(\sqrt{1-u_a^2})}{2L\sigma_n}\left[\int_0^{u_a}\frac{\Phi(t)dt}{\sqrt{(1-t^2)(u_a^2-t^2)}}\right]^{-1}. \tag{3.12}$$

For the calculation of the current density, it is convenient to introduce a complex current,

$$j(z)=j_x-ij_y. \tag{3.13}$$

With the help of Eq. (3.6) Ohm's law can be written as

$$j=-\sigma_n\frac{d\chi}{dz}=\frac{I}{Lb}J(w), \tag{3.14}$$

where

$$J(w)=-\frac{\pi}{4(U-U_0)}\boldsymbol{K}(\sqrt{1-u_a^2})\times\left[\int_0^{u_a}\frac{\Phi(t)dt}{\sqrt{(1-t^2)(u_a^2-t^2)}}\right]^{-1}(1-w^2)\frac{d\chi}{dw}. \quad (3.15)$$

After a quite tedious calculation of $d\chi/dw$, the result is reduced to

$$J(w)=\frac{1}{2}\left[\int_0^{u_a}\frac{\Phi(t)dt}{\sqrt{(1-t^2)(u_a^2-t^2)}}\right]^{-1}\times\sqrt{\frac{1-w^2}{w^2-u_a^2}}[J_1(u_a)-J_2(w,u_a)], \quad (3.16)$$

where

$$J_1(u_a)=\boldsymbol{E}(\sqrt{1-u_a^2})\int_0^{u_a}\frac{\Phi(t_1)dt_1}{\sqrt{(1-t_1^2)(u_a^2-t_1^2)}}-\boldsymbol{K}(\sqrt{1-u_a^2})\int_0^{u_a}\frac{\Phi(t)t^2dt}{\sqrt{(1-t^2)(u_a^2-t^2)}}, \quad (3.17a)$$

$$J_2(w,u_a)=\boldsymbol{K}(\sqrt{1-u_a^2})\int_0^{u_a}\frac{\sqrt{(1-t^2)(u_a^2-t^2)}}{t^2-w^2}\Phi'(t)tdt, \quad (3.17b)$$

where $\boldsymbol{E}(k)$ is the complete elliptic integral of the second kind.

If the resistance of the p-cladding can be neglected (the exact criterion is given in Sec. III B), then $\Phi(t)=1$, $J_2(w,u_a)=0$, and

$$J_1(u_a)=\boldsymbol{K}(u_a)\boldsymbol{E}(\sqrt{1-u_a^2})-[\boldsymbol{K}(u_a)-\boldsymbol{E}(u_a)]\boldsymbol{K}(\sqrt{1-u_a^2})=\frac{\pi}{2}, \quad (3.18)$$

due to the Legendre relation.[24] As a result,

$$J(w)=\frac{\pi}{4\boldsymbol{K}(u_a)}\sqrt{\frac{1-w^2}{w^2-u_a^2}}, \quad (3.19)$$

and the resistance of the structure

$$r=\frac{1}{2L\sigma_n}\frac{\boldsymbol{K}(\sqrt{1-u_a^2})}{\boldsymbol{K}(u_a)}. \quad (3.20)$$

Expression (3.19) has a very remarkable property: it is singular at $w=\pm u_a$. In other words, the current density goes to infinity at the edges of the active region. The reason for this behavior is very simple. It is known that at sharp edges of a charged piece of metal, the electric field goes to infinity. The infinite value of the current density results from the infinite electric field.

The singular behavior of the current at the edges of the active region came from the approximation used in Eq. (3.19). In reality, the current density is singular at the edges of the contact stripe, while at the edges of the active region the singularity is smeared by the resistance of the p-cladding and by a small spread of the current there. The first reason is considered in the next subsection.

B. Potential distribution at the active region

According to Eqs. (3.13) and (3.14) $j_y=-(I/Lb)\mathrm{Im}\,J(w)$. At the active region, $y=0$ and $|x|<a/$; that is, at $v=+0$ and $|u|<u_a$, Eq. (3.16) gives

$$\mathrm{Im}\,J(u+i0)=-\frac{1}{2}\left[\int_0^{u_a}\frac{\Phi(t)dt}{\sqrt{(1-t^2)(u_a^2-t^2)}}\right]^{-1}\times\sqrt{\frac{1-u^2}{u_a^2-u^2}}[J_1(u_a)-\mathrm{Re}\,J_2(u,u_a)]. \quad (3.21)$$

The substitution of this expression in Eq. (3.1) leads to the equation

$$\Phi(u)=1-\frac{b_1\sigma_n}{b\sigma_p}\sqrt{\frac{1-u^2}{u_a^2-u^2}}\left[\frac{J_1(u_a)}{\boldsymbol{K}(\sqrt{1-u_a^2})}-\mathrm{V.p.}\int_0^{u_a}\frac{\sqrt{(1-t^2)(u_a^2-t^2)}}{t^2-u^2}\Phi'(t)tdt\right]. \quad (3.22)$$

We solve Eq. (3.22) with a variational method by minimizing functional

$$\mathcal{F}[\Phi]=\int_{-u_a}^{u_a}\left[\Phi(u)-1-\frac{b_1\sigma_n}{b\sigma_p}\frac{2}{\boldsymbol{K}(\sqrt{1-u_a^2})}\times\int_0^{u_a}\frac{\Phi(t)dt}{\sqrt{(1-t^2)(u_a^2-t^2)}}\mathrm{Im}\,J(u+i0)\right]^2du. \quad (3.23)$$

A good approximation is given by $\Phi(u)=c_1-c_2u^2-c_3u^8$, where c_1, c_2, and c_3 are variational parameters.

The current density resulting from this calculation is presented in Figs. 2 and 3. In Fig. 2, the dependence of the dimensionless current $|J|$ on x/b is given at different distances from the p-contact y/b. The larger this distance, the less pronounced the current singularities are. The active region is at $y/b=0.01$.

In Fig. 3, the dependence of $|J|$ on x/b at $y/b=0.01$ is presented for different ratios of p-cladding and n-layer resistances. It is clearly seen that the resistance of the p-cladding smears the current singularities. Equation (3.22) shows that the effect of p-cladding is controlled by the ratio of the p-cladding and n-layer resistances $b_1\sigma_n/b\sigma_p$. When this ratio is not small, the potential drop across the p-cladding significantly affects the potential distribution.

One also has to keep in mind that there is another factor that smears the current singularity within a small vicinity of the edges of the active region. This is a small current spread in the lateral direction that is neglected in Eq. (3.1). It is easy to show that the ratio of two current components in the p-cladding $j_x/j_y\sim b_1/a\ll 1$. This estimate is not valid, and $j_x/j_y\sim 1$ only at the vicinity on the order of b_1 near the edges. Compared to the finite resistance of the p-cladding that affects the current distribution over the whole width of the active region, the effect of j_x can be neglected.

IV. TEMPERATURE DISTRIBUTION

The calculation of the temperature distribution is reduced to the solution of the equation

$$\frac{\partial^2 T}{\partial x^2}+\frac{\partial^2 T}{\partial y^2}=-\frac{1}{\kappa}Q(x,y), \tag{4.1}$$

in the region $0<y<b$ where T is the temperature excess above the temperature of the heat sink, κ is the thermal conductivity, and $Q(x,y)$ is the dissipated power density. Similar equations with zero on the right-hand side have to be solved in the thermal buffers. The buffers can be modeled by layers with thermal conductivity κ_1 and the width b_2.

In this article, we are interested only in the temperature distribution inside the laser structure, and will disregard the lateral heat spread in the buffer layer (this spread is considered elsewhere[3]). In this case, the temperature derivatives normal to the interface $y=0$ or $y=b$ inside the buffer are $T(x,0)/b_2$ and $T(x,b)/b_2$, respectively, and the respective heat fluxes are $-\kappa_1 T(x,0)/b_2$ and $\kappa_1 T(x,b)/b_2$. The heat flux at any interface is continuous, giving the boundary conditions

$$\left.\frac{\partial T}{\partial y}\right|_{y=0}=\frac{\gamma}{b}T|_{y=0}, \quad \left.\frac{\partial T}{\partial y}\right|_{y=b}=-\frac{\gamma}{b}T|_{y=b}, \tag{4.2}$$

where $\gamma=b\kappa_1/b_2\kappa$ is ratio of thermal resistances of the laser structure and the thermal buffer. In general, γ includes the thermal resistance of the solder layer. Its value also can be modified in the case of a nonideal heat sink.

The solution to Eq. (4.1) with boundary conditions (4.2) can be written in the form

$$T(x,y)=\frac{1}{\kappa}\int_{-\infty}^{\infty}dx'\int_0^b dy' G\left(\frac{x-x'}{b},\frac{y}{b},\frac{y'}{b}\right)Q(x',y'), \tag{4.3}$$

where the Green function is

$$G(\xi,\eta,\eta')=\sum_{n=1}^{\infty}\frac{b}{2\mu_n}e^{-\mu_n|\xi|}Y_n(\eta)Y_n(\eta'), \tag{4.4}$$

$$Y_n(\eta)=B_n\cos\left(\mu_n\eta-\frac{\delta_n}{2}\right), \quad B_n^2=\frac{2}{b}\frac{\mu_n^2+\gamma^2}{\mu_n^2+\gamma^2+2\gamma}, \tag{4.5}$$

and the eigenvalues can be represented as $\mu_n=(n-1)\pi+\delta_n$, $n=1,2,\ldots$, where δ_n is the root of the equation

$$\tan\frac{\delta_n}{2}=\frac{\gamma}{(n-1)\pi+\delta_n}, \tag{4.6}$$

in the interval $(0,\pi)$.

There are three main sources of heat: the active region source $Q_a(x,y)$, the p-cladding source $Q_p(x,y)$, and the n-cladding and substrate source $Q_n(x,y)$. Respectively, there are three contributions to the temperature: $T_a(x,y)$, $T_p(x,y)$, and $T_n(x,y)$. The total temperature rise is

$$T(x,y)=T_a(x,y)+T_p(x,y)+T_n(x,y). \tag{4.7}$$

When comparing the different contributions, it is instructive to pay attention to two features. The first is their dependence on $b_1/b\ll 1$. The higher the power of this parameter, the smaller the heating. The second feature is the fall-off of $T(x,b_1)$ away from the active region that characterizes the mutual heating of different laser stripes in a bar.

A. Heating by the active region

An important feature of $Q_a(x,y)$ is that, due to $b_1\ll a$, the spread of the current between the p-contact and the active region can be neglected, that is, $Q_a(x,y)$ is zero when $|y|>a/2$. Above threshold, the voltage across the active region (U_0) is constant, so that the electric power dissipated in the active region per unit volume is $U_0 j_y\delta(y-b_1)$. Assuming the optical power per unit area of the stripe is $p=\eta_d(j_y-j_{\rm th})$ (η_d is the differential efficiency and $j_{\rm th}$ is the threshold current density), we have

$$Q_a(x,y)=[U_1 j_y(x,b_1)+p_{\rm th}]\times\delta(y-b_1)\theta(a/2-x)\theta(a/2+x), \tag{4.8}$$

where $U_1=U_0-\eta_d$ and $p_{\rm th}=\eta_d j_{\rm th}$. In integral (4.5), $G(x,y,y')$ is simplified, and

$$T_a(x,y)=\frac{U_1 I}{L\kappa}\Theta_{a1}(x/b,y/b)+\frac{p_{\rm th}b}{\kappa}\Theta_{a2}(x/b,y/b), \tag{4.9a}$$

$$\Theta_{a1}(\xi,\eta)=-\int_{-a/2b}^{a/2b}G(\xi-\xi',\eta,b_1/b)\,{\rm Im}\,J\left(\tanh\frac{\pi(\xi'+ib_1/b)}{2}\right)d\xi', \tag{4.9b}$$

$$\Theta_{a2}(\xi,\eta)=\int_{-a/2b}^{a/2b}G(\xi-\xi',\eta,b_1/b)\,d\xi'. \tag{4.9c}$$

The second term in Eq. (4.9a) is the temperature rise due to power dissipated by the threshold current, while the first term comes from the dissipation produced by the current above threshold. The dependence of Θ_{a1} and Θ_{a2} on x/b at the level of y corresponding to the active region is shown in Figs. 4 and 5.

B. Heating by *p*-cladding

Due to negligible current spread in the p-cladding, Eq. (3.14) gives

$$Q(x,y)=\begin{cases}\dfrac{I^2}{L^2b^2\sigma_p}\left|J\left(\tanh\dfrac{\pi z}{2b}\right)\right|^2, & \text{if } |x|<a/2, 0<y<b_1,\\ 0, & \text{otherwise.}\end{cases} \tag{4.10}$$

Equation (4.5) takes the form

$$T_p(x,y)=\frac{I^2}{L^2\sigma_p\kappa}\Theta_p(x/b,y/b), \tag{4.11a}$$

$$\Theta_p(\xi,\eta)=\int_{-a/2b}^{a/2b}d\xi'\int_0^{b_1/b}d\eta' G(\xi-\xi',\eta,\eta')\times\left|J\left(\tanh\frac{\pi(\xi'+i\eta')}{2}\right)\right|^2. \tag{4.11b}$$

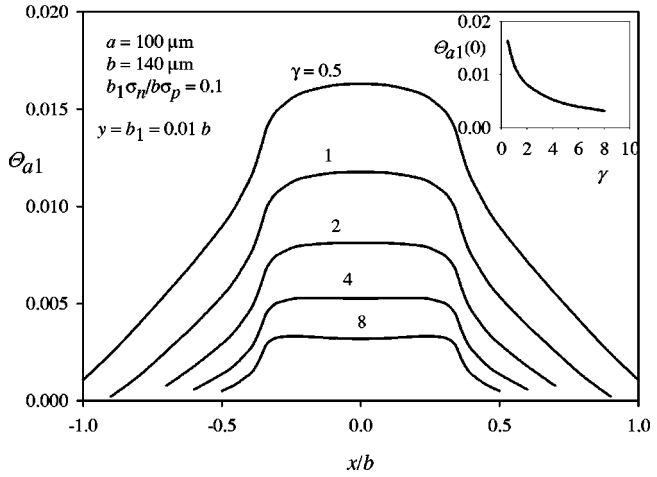

FIG. 4. The dimensionless temperature created by the above threshold current across the active region as a function of x/b at the level of the active region. The labels on the curves give the ratio γ of the thermal resistances of the structure and the thermal buffer. The inset shows the dependence of Θ_{a1} at $x=0$ as a function of γ.

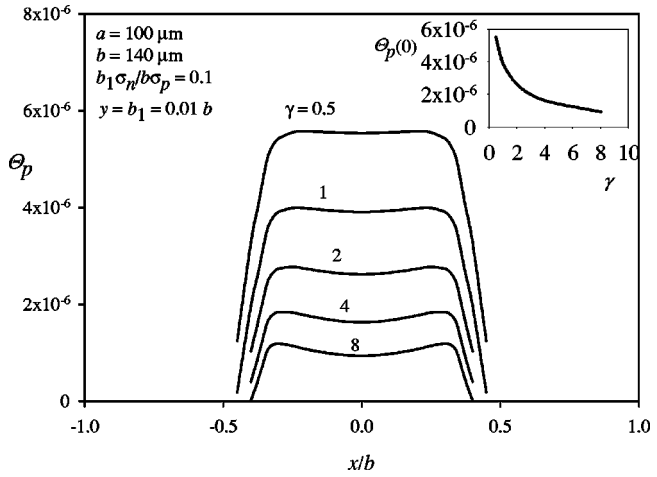

FIG. 6. The dimensionless temperature created by the series resistance of p-cladding as a function of x/b at the level of the active region. The labels on the curves give the ratio of the thermal resistances of the structure and the thermal buffer (γ). The inset shows the dependence of Θ_p at $x=0$ as a function of γ.

The dependence of Θ_p on x/b at the level of y corresponding to the active region is shown in Fig. 6.

C. Heating by *n*-cladding and substrate

In this region, the heat source is

$$Q_n(x,y)=\begin{cases}\dfrac{I^2}{L^2b^2\sigma_n}\left|J\left(\tanh\dfrac{\pi z}{2b}\right)\right|^2, & b_1<y<b,\\ 0, \quad \text{otherwise.}\end{cases} \tag{4.12}$$

The contribution of the thin p-cladding, $0<y<b_1$, is relatively small and can be neglected. As a result,

$$T_n(x,y)=\frac{I^2}{L^2\sigma_n\kappa}\Theta_n(x/b,y/b), \tag{4.13a}$$

$$\Theta_n(\xi,\eta)=\int_{-\infty}^{\infty}d\xi'\int_{b_1/b}^{1}d\eta'\,G(\xi-\xi',\eta,\eta')\times\left|J\left(\tanh\frac{\pi(\xi'+i\eta')}{2}\right)\right|^2 \tag{4.13b}$$

The dependence of Θ_n on x/b at the level of y corresponding to the active region is shown in Fig. 7.

V. RESULTS

The first important result that we obtained is a description of the nonuniform current distribution in the active region. The current singularities near the edges of the active region (Fig. 3) can substantially affect the mode composition

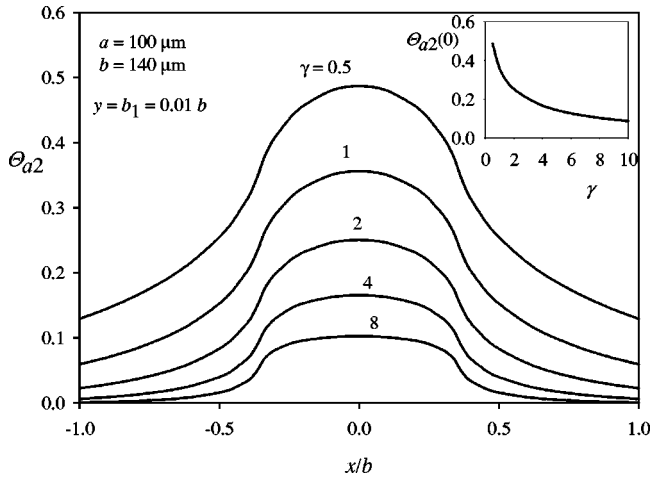

FIG. 5. The dimensionless temperature created by the threshold current across the active region as a function of x/b at the level of the active region. The numbers on the curves give the ratio of the thermal resistances of the structure and the thermal buffer (γ). The inset shows the dependence of Θ_{a2} at $x=0$ as a function of γ.

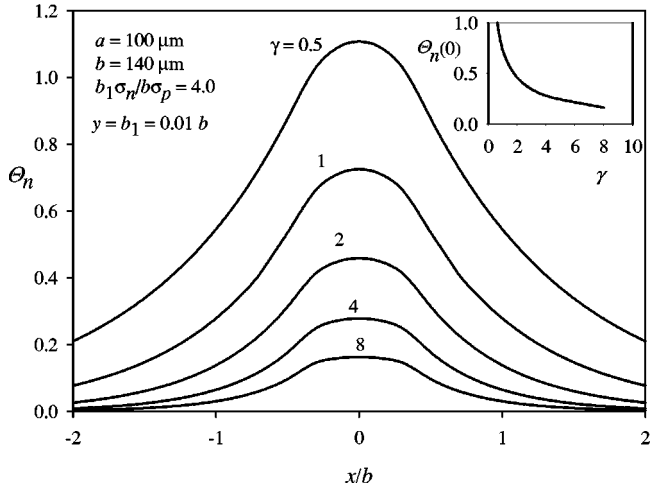

FIG. 7. The dimensionless temperature created by the series resistance of the n-layer as a function of x/b at the level of the active region. (a) and (b) correspond, respectively to different values of the ratio of the p-cladding and n-layer resistances, $b_1\sigma_n/b\sigma_p$. The labels on the curves give the ratio γ of the thermal resistances of the structure and the thermal buffer. The inset shows the dependence of Θ_n at $x=0$ as a function of γ.

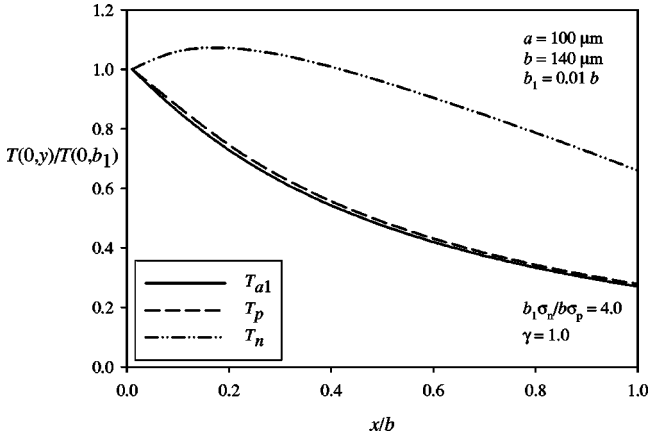

FIG. 8. The profile of different contributions to the temperature across the n-layer. T_{a1} and T_{a2} cannot be distinguished. Contrary to all others, T_n has a maximum in the middle of n-region.

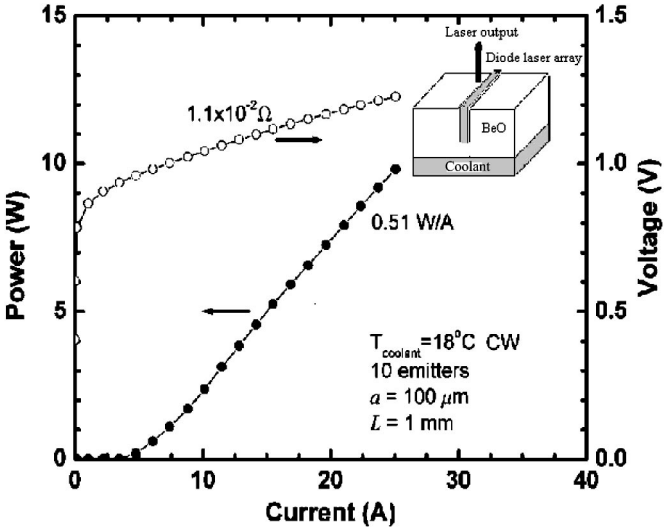

FIG. 9. Measured output power and wall-plug efficiency of a 10-emitter laser bar versus current. The inset shows how the laser bar was mounted on the heat sink.

of the generated light. In this article, we do not study this effect, and are concerned only with the nonuniform heating of the active region.

The temperature in the structure is represented as

$$T(x,y)=\frac{p_{\mathrm{th}}b}{\kappa}\Theta_{a2}\left(\frac{x}{b},\frac{y}{b}\right)+\frac{U_1 I}{L\kappa}\Theta_{a1}\left(\frac{x}{b},\frac{y}{b}\right)+\frac{I^2}{L^2\sigma_p\kappa}\Theta_p\left(\frac{x}{b},\frac{y}{b}\right)+\frac{I^2}{L^2\sigma_n\kappa}\Theta_n\left(\frac{x}{b},\frac{y}{b}\right), \tag{5.1}$$

where the first term is the heating in the active region due to the threshold current, the second term is the heating in the active region due to the current above threshold, and last two terms come from the heating by the p-cladding and n-layer series resistances, respectively. The dimensionless functions $\Theta_{a2}(x/b,y/b)$, $\Theta_{a1}(x/b,y/b)$, $\Theta_p(x/b,y/b)$, and $\Theta_n(x/b,y/b)$ describe the coordinate dependence of the temperature and are represented in Figs. 4–8. Typically, the temperature of the active region is nearly proportional to the current,[3,12,25,26] which means that the main heat source is the power dissipation in the active region.

The edges of the active region can be heated more strongly than the middle at a relatively small p-cladding layer resistance (Figs. 4 and 6) when the current singularity at the edges is strong enough (see Fig. 3).

The temperature distribution in the active region depends substantially on the ratio of the thermal resistances of the structure and buffer layer (γ). For a small γ (i.e., relatively large thermal resistance of the buffer layer), the thermal exchange between the structure and the heat sink is hindered. Thus, a wider region of the interface is needed to transfer the heat generated in the structure to the heat sink. When this region is wider than the active region, a significant part of the heat flux from the active region goes in the lateral direction. As a result, the edges of the active region have better cooling conditions and their temperature is lower. At large γ, the heat flux is directed perpendicular to the interface, and cooling conditions of all parts of the active region are more or less the same. As a result, the temperature is higher in the places where more heat is generated; that is, at the edges. These details are reflected in Figs. 4 and 6.

The spread of the heat generated in the active region and p-cladding in the lateral direction away from the active region is relatively weak. This results from the relatively short distance between the active region and the boundary of the structure. One has to keep in mind that the model we used here considers only the lateral heat flow in the laser bar. If the thickness of the buffer layer is large compared to the laser structure, most of the lateral spread takes place in the buffer layer. The situation is different for the heat generated in the n-layer. It can spread at the distance about the thickness of the layer before it is transferred to the heat sinks. Typically, however, the amount of this heat is very small and its effect on the lateral heat spread is negligible.

The heat generated in p-cladding and the active layer is transferred to the heat bath mainly via the p-side just because the thickness of p-cladding is significantly smaller than that of n-layer resulting in a smaller thermal resistance. The profile of the different contributions to the temperature across the structure is shown in Fig. 8. The power dissipated in the n-layer leads to a maximum of the contribution in the middle of the layer, contrary to the others.

We compared the theoretical results with measurements made on laser bars mounted in metallized grooves in BeO blocks which were bonded on a water-cooled microchannel Cu heat sink (see inset in Fig. 9). The InGaAsP/InP heterostructure was grown by metalorganic chemical vapor deposition. The active region consisted of three 6-nm-thick compressively strained QWs incorporated into a two-step graded index waveguide with a total thickness of 710 nm. Zn doping of the 1.5-μm-thick p-cladding provided optical loss as low as $2-3\ \mathrm{cm}^{-1}$.[27,28] The separation between n- and p-contacts was 140 μm. The laser facets were high-reflection/anti-reflection coated with reflection coefficients of 95% and 3%, respectively. We used a 1-cm-long laser bar containing ten 100-μm-wide emitters equally spaced 1 mm center-to-center.

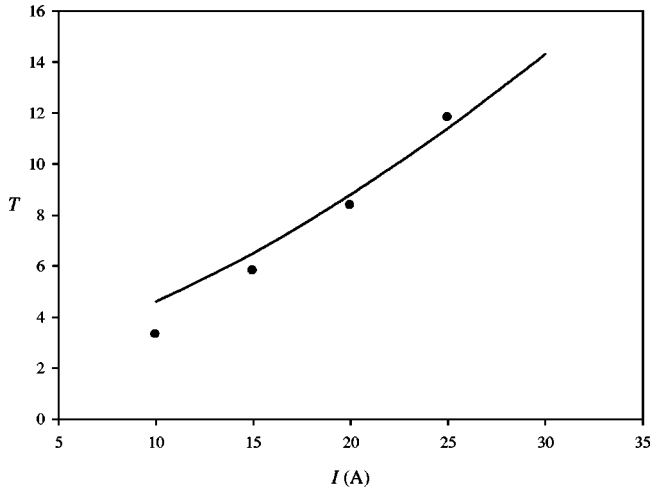

FIG. 10. Temperature of the active region versus current. Points present the measured temperature and the curve gives the theoretical dependence.

The laser cavities were 1 mm long. The laser power versus current is presented on Fig. 9. The measured resistance is consistent with $\sigma_n = 320\ \Omega^{-1}\ \mathrm{cm}^{-1}$ and $\sigma_p = 1.6\ \Omega^{-1}\ \mathrm{cm}^{-1}$. The voltage across the active region $U_0 = 0.91$ V. The power dependence on the current gives efficiency $\eta_d = 0.51$ W/A and the threshold current for one emitter is 0.5 A.

The temperature of the laser active region was estimated from the emission spectrum shift with drive current. To calculate the temperature change a calibration factor of 0.55 nm/K was obtained by measuring the spectral shift under low-duty-cycle (0.02%), low-pulse-width (200 ns) excitation at a variety of heat-sink temperatures.[29] To estimate the contribution of factors related to current change, we fixed the heat-sink temperature and increased the current in low-duty-cycle pulse operation. The spectral shift due to current under these conditions was insignificant. We conclude that the observed redshift under cw and quasi-cw operation is due to heating in the active region. For the theoretical calculation of the temperature we took the thermal resistance of BeO as that of a plane layer of 830 μm width (see Ref. 3). This corresponded to the ratio of the thermal resistances of the laser structure and the buffer layer $\gamma = 0.62$.

We did not consider a longitudinal nonuniformity of the temperature in the cavity.[4,5,9] In other words, we assumed that the pumping current is uniform along the cavity and the measured temperature is an average of the temperature distribution along the cavity. Agreement between the theoretical and experimental results can be seen from Fig. 10. Our calculation shows that at the current $I = 20$ A, the temperature near the edges of the active region is lower than the temperature in the middle by about 2°. At this current, 50% of the heating comes from the active region. With an increase in current, the role of the active region diminishes. To estimate the importance of the nonuniform lateral current distribution, we calculated this contribution also for the uniform lateral current distribution. In this case, the heating in the middle of the active region appears nearly two times larger, and the difference between the heating in the middle and near the edges is about 30%. This is understandable because for the nonuniform lateral current distribution, most of the current flows more close to the edges of the active region where the cooling is better.

VI. CONCLUSION

The results of the calculation allow us to make the following conclusions.

- The current is nonuniformly distributed laterally across the active region. The smaller the thickness of p-cladding and the larger its conductivity, the larger the magnitude of the current density near the edges of the active region compared to the middle.
- The nonuniform current distribution across the active region can (i) affect the optical energy distribution between high- and low-order modes and (ii) lead to a higher temperature at the edges of the active region than in the middle.
- Heat spread in the lateral direction comes mainly from the current spread and the heat conductance in the relatively thick n-substrate. The width of the lateral spread in the n-layer is about the thickness of this layer. Due to the relatively small contribution of the heat dissipated in the n-layer, significant lateral heat spread and mutual heating of lasers in a bar takes place in the buffer layers.
- The thermal resistance of the buffer layers crucially affects the heating of the active region and the lateral width of the temperature distribution.
- The active region edges may experience higher than expected temperatures, which could have implications for the device lifetime. This may be especially important near the facets where additional heat loads are applied.

ACKNOWLEDGMENT

The work was supported by Grant of Army Research Office DAAD 190010423 and MURI Air Force Office of Scientific Research: F49620-00-1-0331.

[1] S. O'Brien, H. Zhao, and R. J. Lang, Electron. Lett. **34**, 184 (1998).
[2] M. Maiorov, R. Menna, V. Khalfin, H. Milgazo, R. Matarese, D. Garbuzov, and J. Connolly, IEEE Photonics Technol. Lett. **11**, 961 (1999); M. Maiorov, R. Menna, V. Khalfin, H. Milgazo, A. Triano, D. Garbuzov, and J. Connolly, Electron. Lett. **35**, 636 (1999).
[3] A. Gourevitch, G. Belenky, D. Donetsky, B. Laikhtman, D. Westerfeld, C. W. Trussell, H. An, Z. Shellenbarger, and R. Martinelli, Appl. Phys. Lett. (to be published).
[4] U. Menzel, Semicond. Sci. Technol. **13**, 265 (1998).
[5] G. Chen and C. L. Tien, J. Appl. Phys. **74**, 21672174 (1993).
[6] C. H. Henry, P. M. Petro., R. A. Logan, and F. R. Merritt, J. Appl. Phys. **50**, 3721 (1979).
[7] K. P. Pipe, R. J. Ram, and A. Shakouri, IEEE Photonics Technol. Lett. **14**, 453 (2002); Phys. Rev. B **66**, 125316 (2002).
[8] W. Nakwaski, IEEE J. Quantum Electron. **QE 21**, 331 (1988).
[9] G. Erbert, A. Bärwolff, J. Sebastian, and J. Tomm, in *High-Power Diode Lasers*, edited by R. Diehl, Lasers, Topics Appl. Phys. Vol. **78** (Springer, Berlin, 2000), p. 173.
[10] R. P. Sarzala and W. Nakwaski, J. Therm. Anal. **36**, 1171 (1990); **39**, 1297 (1993).
[11] A. Bärwolff, R. Puchert, P. Enders, U. Menzel, and D. Ackermann, J. Therm. Anal. **45**, 417 (1995).
[12] U. Menzel, A. Bärwolff, P. Enders, D. Ackermann, R. Puchert, and M. Voss, Semicond. Sci. Technol. **10**, 1382 (1995).

[13] H. Yonezu, I. Sakuma, K. Kobayashi, T. Kamejima, M. Ueno, and Y. Nannichi, Jpn. J. Appl. Phys. **12**, 1585 (1973).
[14] W. P. Dumke, Solid-State Electron. **16**, 1279 (1973).
[15] J. Buus, IEEE J. Quantum Electron. **QE-15**, 734 (1979).
[16] W. Streifer, R. D. Burnham, and D. R. Scifres, IEEE J. Quantum Electron. **QE-18**, 856 (1982).
[17] W. B. Joyce and S. W. Wemple, J. Appl. Phys. **41**, 3818 (1970); W. B. Joyce and R. W. Dixon, *ibid.* **46**, 856 (1975).
[18] G. Lengyel, P. Meissner, E. Patzak, and K.-H. Zschauer, IEEE J. Quantum Electron. **QE-18**, 618 (1982).
[19] D. P. Wilt and A. Yariv, IEEE J. Quantum Electron. **QE-17**, 1941 (1981).
[20] W. B. Joyce, J. Appl. Phys. **51**, 2394 (1980).
[21] G. P. Agrawal, J. Appl. Phys. **56**, 3100 (1984).
[22] R. Papannareddy, W. E. Ferguson, Jr., and J. K. Butler, IEEE J. Quantum Electron. **QE-24**, 60 (1988).
[23] F. D. Gakhov, *Boundary Value Problems* (Dover, New York, 1966).
[24] E. T. Whittaker and G. N. Watson, *A Course of Modern Analysis* (Cambridge University Press, Cambridge, 2002).
[25] S. R. Chin, P. D. Zory, and A. R. Reisinger, IEEE J. Quantum Electron. **QE 24**, 2191 (1988).
[26] R. Beach, W. J. Benett, B. L. Freitas, D. Mundinger, B. J. Comaskey, R. W. Solarz, and M. A. Emanuel, IEEE J. Quantum Electron. **28**, 966 (1992).
[27] L. Shterengas, R. Menna, C. W. Trussell, D. Donetsky, G. Belenky, J. Connolly, and D. Garbuzov, J. Appl. Phys. **88**, 2211 (2000).
[28] G. Belenky, L. Shterengas, C. W. Trussell, C. L. Reynolds, M. S. Hybertsen, and R. Menna, in *Future Trends in Microelectronics*, edited by S. Luryi, J. Xu, and A. Zaslavsky (Wiley, New York, 2002) pp. 230–241.
[29] Landolt-Börnstein, *Numerical Data and Functional Relationships in Science and Technology* (Springer, New York, 1982), Vol. 17.